Dyes and Pigments 80 (2009) 212–218

Contents lists available at ScienceDirect

Dyes and Pigments

journal homepage: www.elsevier.com/locate/dyepig

Supramolecular architecture, spectroscopic properties and stability of C.I. Basic Violet 10 (Rhodamine B) at high concentration

Xiao Zhao, Shuxue Zhou, Min Chen, Limin Wu*

Department of Materials Science, Advanced Coatings Research Center of the Ministry of Education of China, Advanced Materials Laboratory, Fudan University, Shanghai 200433, PR China

ARTICLE INFO

Article history:
Received 14 April 2008
Received in revised form 30 June 2008
Accepted 1 July 2008
Available online 18 July 2008

Keywords:
Rhodamine B
Self-assembly
Nanocrystals
Stability
Supramolecular architecture
Nanorod

ABSTRACT

The self-assembly behavior, spectroscopic properties and stability of C.I. Basic Violet 10 (Rhodamine B) were investigated at a relatively high concentration. Rod-like dye nanocrystals could be formed by tuning various THF/H_2O volume ratios, leading to increased fluorescence intensity. TEM, zeta-potential measurement and selected-area electron diffraction patterns indicated that the dye nanorods were successfully encapsulated within a silica layer using a sol–gel process. The ensuing silica-coated, dye nanorods exhibited increased fluorescence intensity, non-leachability in polar solvents and high photostability.

1. Introduction

Dyes such as xanthene, cyanine and azo are traditionally used as colorants, as laser materials and as biological probes in many commercial products [1]. Dyes also exhibit diverse optical or electro-optical properties with potential applications in novel devices, e.g., non-linear optical devices [2–5], nano-scale semi-conductor devices [6] and photorefractive applications [7].

It is well known that dye molecules tend to form supramolecular architectures via self-assembly in solution or in adsorbed states [8–15]. For example, Tian et al. [3,16] fabricated low-dimensional nanorods and nanospheres of a stilbazolium-like organic dye with highly monodisperse size using a self-assembly method. They found that the functions of the materials depended on the size and shape. Using dipolar aggregation of merocyanine dyes, Horn and Rieger [4] successfully obtained well-organized helical nanorods. Gesquiere and colleagues [17] prepared disk-like nanoparticles of *N*,*N*′-bis(2,5-di-*tert*-butylphenyl)-3,4,9,10-perylene-dicarboximide of uniform size by a reprecipitation method.

However, due to the weak non-covalent interactions including hydrogen bonds, aromatic π stacking, electrostatic and van der Waal's interactions, the formed supramolecular complexes are usually in equilibrium with their component parts and other undesired complexes. As a consequence, the desired supramolecular architectures have a low yield as well as low stability upon environmental change. To solve this problem, incorporation of dyes into a silica matrix or Si–Ti binary oxide matrix via a sol–gel method is frequently adopted to tailor and stabilize the supramolecular architectures or to exhibit higher fluorescent intensity and higher photostability of C.I. Basic Violet 10 (Rhodamine B; RB) or C.I. Basic Red 1 (Rhodamine 6G; R6G) [18–25]. For example, Avnir et al. [18] embedded R6G molecules in thin silica-glass films and found that undesired aggregation could be avoided because of the cage effect. A red fluorescence shift occurred owing to the rigid cage, and the R6G encapsulated within silica glass also exhibited better photostability. Del Monte and colleagues [19–22] fabricated RB dimers on the porous surface of silica gels and RB nanoparticles by entrapping RB molecules in γ-glycidyloxypropyl trimethoxysilane (GPTMS)-based sol–gel glass. They found that the formation of larger nanoparticles led to fluorescence enhancement. In addition, intercalation of dye molecules into layered inorganic solids could also produce ordered dye molecular aggregates [26–28].

Most of the aforementioned studies were carried out at extremely low concentrations (e.g., 10^{-4} M or even much lower) to avoid undesired aggregates, which would influence the expected electro-optic response. Up to now, very few studies have focused on the aggregation behavior and performance of organic dyes at high concentrations. In the present study, we took RB as an example and investigated the self-assembly behavior, spectroscopic properties

* Corresponding author. Tel./fax: +86 21 65643795.
E-mail address: lmw@fudan.edu.cn (L. Wu).

0143-7208/$ – see front matter © 2008 Elsevier Ltd. All rights reserved.
doi:10.1016/j.dyepig.2008.07.003

and stability of RB dispersions at comparatively high concentration by tuning the volume ratio of tetrahydrofuran (poor solvent) to H_2O (good solvent) to obtain RB nanorod structures at high concentration. To stabilize the formed organic nanostructure, it was further encapsulated within silica using a sol–gel process. The resulting RB product exhibits strong excited fluorescent emission, non-leachability in polar solvents and good photostability.

2. Experimental section

2.1. Materials

Rhodamine B (RB, analytical grade), tetrahydrofuran (THF, analytical grade), tetraethyl orthosilicate (TEOS) and acetic acid (CH_3COOH) were obtained from Sinopharm Group Chemical Reagent Co., Ltd. (China). γ-Glycidyloxypropyl trimethoxysilane (GPTMS) was purchased from Dow Corning. All chemicals were used as received. Double-distilled deionized water was used for preparation of solutions.

2.2. Preparation of RB aggregates

To obtain well-ordered dye architectures, RB was dissolved in a mixture of water (good solvent) and THF (poor solvent) at different volume ratios (THF/H_2O from 1:6 to 6:1). The typical process was carried out as follows: 0.26 g of RB powder was dissolved in 7.8 ml of water by magnetic stirring for 10 min. Then 46.8 ml of THF was injected and stirred for another 150 min, resulting in an RB dispersion of 1×10^{-2} M in 6:1 (v/v) THF/H_2O. Similarly, RB dispersions of the same concentration in 1:6 and 1:1 THF/H_2O were prepared by altering the relative amounts of water and THF. The RB dispersions obtained were denoted as RB-61, RB-11 and RB-16 for THF/H_2O volume ratios of 6:1, 1:1 and 1:6, respectively.

An aqueous RB solution of 1×10^{-2} M was prepared by directly dissolving 0.26 g of RB powder in 55 ml of water. Both the aqueous RB solution and the dispersion of 1×10^{-2} M were diluted to 1×10^{-5} M for comparison purposes.

2.3. Encapsulation of RB aggregates into silica

The RB-61 dispersion was further incubated with a mixture of TEOS (1.8 ml), GPTMS (1.78 ml), THF (1.81 ml) and CH_3COOH (1 ml) for a period of 150 min at room temperature to allow encapsulation in silica. The dispersion obtained was kept at a concentration of 1×10^{-2} M (RB-61Si) and aged in the dark for 24 h before measurements were performed.

2.4. Characterization

UV–vis spectra: absorption spectra were recorded on a UV–vis spectrophotometer (Hitachi UV-3000, Japan) at a temperature of 25 ± 1 °C.

TEM and SAED observations: a transmission electron microscope (TEM; Hitachi H-600, Hitachi, Japan) was used to observe the morphology of RB aggregates. The RB dispersions were dropped onto carbon-coated copper grids and dried at room temperature before examination. Selected-area electron diffraction (SAED) was performed on a JEM 200 CX microscope operated at 160 kV.

SEM observations: a scanning electron microscope (SEM; Philips XL30 apparatus) was used to observe morphological features. One drop of RB dispersion was coated onto aluminum foil and then spun at 5000 rpm for 30 s to produce a film for observation. The film obtained was sputter-coated with gold prior to examination.

pH value: pH value was measured with a digital pH meter (Model PHS-25, Ingold Instrument CO., Ltd., Shanghai, China) at room temperature.

Zeta potential: the zeta potential was measured at 30 runs per analysis using a zeta-potential analyzer (Zetasizer, Model Nano-ZS, Malvern Instrument, UK) at 25 °C.

Leachability measurement: an aliquot of 0.5 ml of aged sol was dip-coated onto cleaned glass (1×1 cm^2) to produce sol–gel thin films. The films were aged and dried in the dark for 7 days. Doped glasses were immersed into four different leaching solvents: H_2O, HCl (0.1 M, pH 1), ethanol and NaOH (0.1 M, pH 13). The absorption spectra and appearance of the leachates were observed to evaluate the leachability.

Emission spectra: the fluorescence emission intensity was measured for all samples with excitation at 560 nm on an FLS 920 spectrophotometer (Edinburgh Instruments, Livingston, UK) immediately after sample preparation.

UV irradiation: photodecomposition was carried out by placing samples in a UV crosslinker with five 8-W UV-C tubes (wavelength 365 nm, 3.1 mW/cm^2, Model XLE-1000, Spectroline, USA). After UV irradiation, the emission intensity was measured as a function of the UV irradiation time. The ratio of I_t/I_0 was adopted to evaluate the photostability of RB, where I_t denotes the height of emission

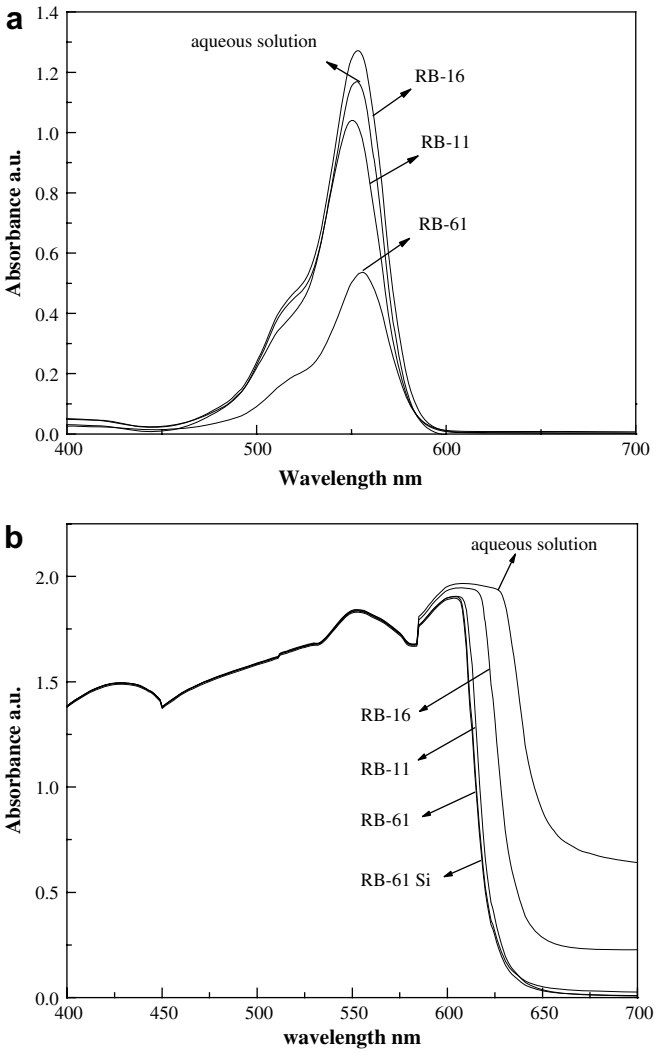

Fig. 1. Effect of THF/H_2O ratios on the absorption spectra of RB solutions and dispersions. (a) 1×10^{-5} M, and (b) 1×10^{-2} M (cell length: 1 mm).

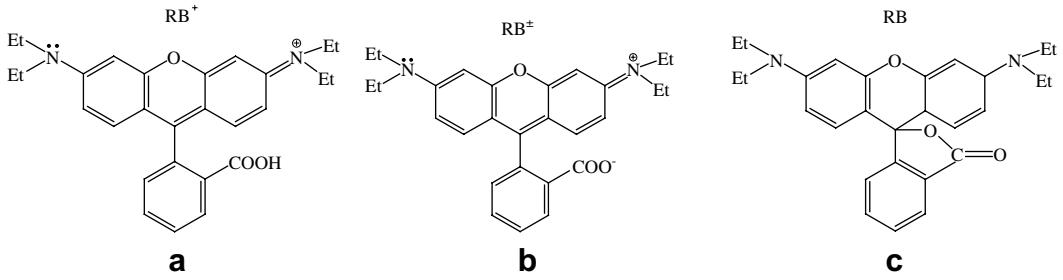

Fig. 2. Molecular structure of Rhodamine B equilibrium species.

peak of the sample at UV irradiation time t and I_0 is the emission peak of the sample before UV irradiation.

3. Results and discussion

3.1. UV–vis absorption spectra

Mixtures of a good solvent (water) and a poor solvent (THF) for RB at different volume ratios cause RB aggregation of various degrees. Fig. 1 demonstrates the effect of the THF/H_2O ratio on the visible absorption spectra of RB solutions and dispersions at 10^{-5} and 10^{-2} M, respectively. At low concentration (10^{-5} M, pH value ≈ 2.5), the spectrum of aqueous RB solution has an absorption peak at ~553 nm and a shoulder at ~506 nm (Fig. 1a), indicating that this solution only contains monomer and dimer [9]. The RB-16 dispersion had higher absorption intensity than the aqueous solution, but the intensity decreased with increasing THF/H_2O ratio. Moreover, the position of the peak maximum also shifted with THF/H_2O ratio, with a 3-nm blue shift for RB-11 and a 3-nm red shift for RB-61.

Both the intensity change and band shift could be explained by solvent effects on solute–solvent interactions and the structure of RB molecules in solution and dispersions. The RB molecule can exist in acid (RB^+) or in zwitterion form ($RB^{\pm}$) in polar solvents, as indicated in Fig. 2, and the cations tend to interact with anions in aqueous solutions [29–32]. As a result, dimers can be formed via electrostatic and van der Waals' forces. Hydrogen bonding is another major driving force for the formation of RB dimers in aqueous solution. However, addition of a small amount of nonpolar THF altered the separation of charges in solution and weakened the hydrogen bonds between water and dye molecules, which caused disaggregation of dimers. Thus, the comparatively high monomer concentration with high oscillatory strength should contribute to the slight increase in intensity for RB-16. As more THF was added, a large positive entropy of solvation increased the system disorder, inducing the reorientation of dipole moments, a process that could be influenced by the THF/H_2O volume ratio. At a THF/H_2O ratio of 1:1, intramolecular interaction between $-COO^-$ and the xanthene ring increased due to solvophobic effects and a new equilibrium shift to dimer formation was established again, which could explain the decrease in absorption intensity and the blue shift of the absorption peak for sample RB-11. When the THF content was further increased (THF/H_2O, 6:1), most of the RB molecules existed in the form of a lactone (Fig. 2). Since lactones are colorless and cannot contribute to the absorption spectrum, an obvious decrease in intensity is unavoidable in this solvent environment. In addition, closing of the lactone ring means that intramolecular interactions no longer occur in the system, leading to a red shift of the monomer peak in THF-rich solution.

The absorption spectra of RB solution and dispersions at high concentration (10^{-2} M, pH value ≈ 6.5) shown in Fig. 1b are quite different from those in dilute systems. A new peak at lower energy appeared at 626 nm, which might be attributed to the formation of trimers and polymers [9]. Owing to the existence of trimers and polymers at high concentration, the effect of solvent composition on the absorption spectra differed greatly compared to the effect in very dilute systems. Fig. 1b reveals that as the amount of THF increased, the maximum position of the peak at 626 nm gradually blue-shifted, the absorption band narrowed, and the absorption intensity decreased. The spectrum of RB-61Si is also presented in Fig. 1b and shows that the sol–gel process had no impact on the peak shape or intensity.

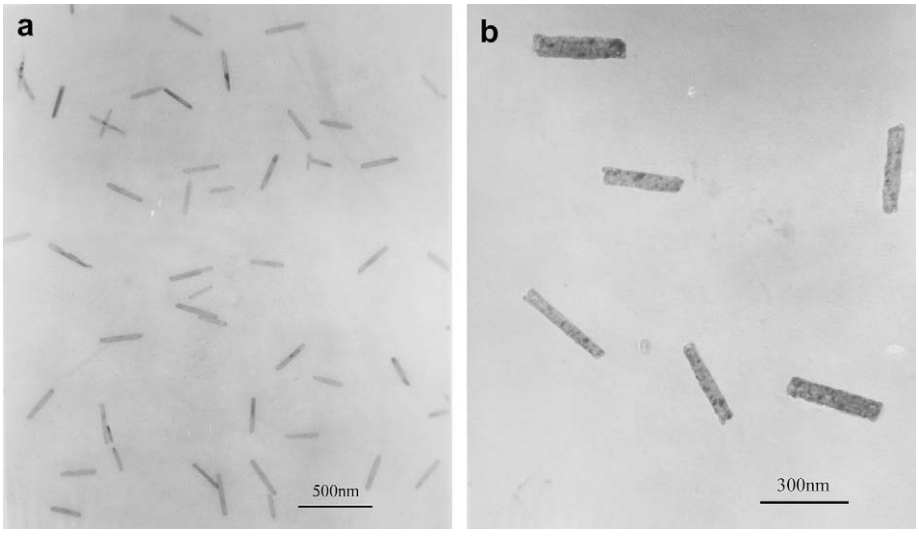

Fig. 3. TEM images of sample RB-61 (1×10^{-2} M) with various magnifications, a and b are TEM and SEM images of the same sample (RB61).

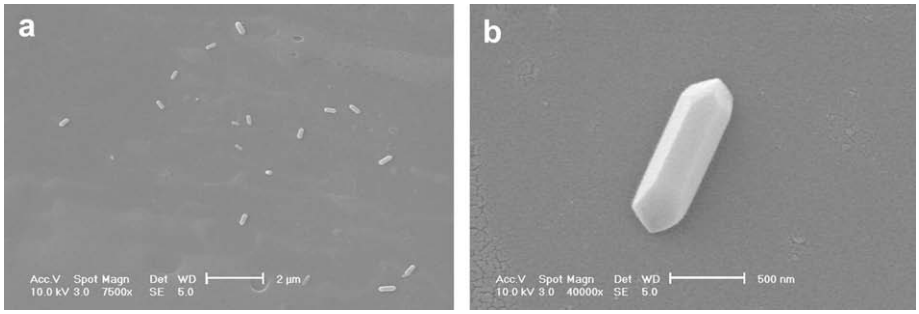

Fig. 4. SEM images of sample RB-61 with various magnifications, a and b are TEM and SEM images of the same sample (RB61).

Similar to the spectral shift for RB dispersions at 10^{-5} M, addition of THF to RB dispersions at 10^{-2} M led to an increase in intramolecular interactions, inducing reorganization of the dipole moments and further driving the formation of well-defined aggregates, resulting in a blue shift of the peak maximum. However, the red shift apparent in the dilute system was not observed. This difference is attributed to the presence of only acid and zwitterion forms at high RB concentration, which was further confirmed by a decrease in pH for RB dispersions from ~6.5 at 10^{-5} M to 2.5 at 10^{-2} M.

3.2. Morphology and structure of RB aggregates

According to the absorption results for RB dispersions, the THF/H_2O ratio can affect the aggregation of RB molecules. Therefore, we used electron microscopes to observe the morphology of RB aggregates as a function of the THF/H_2O ratio. The formation of nanorods was observed for a THF/H_2O volume ratio greater than 3:1. For example, at a THF/H_2O ratio of 6:1, nanorods of perfect uniform size and shape were obtained, as illustrated in Fig. 3. The average length of the nanorods is ~300 nm and the diameter is ~50 nm. SEM images of these nanorods are presented in Fig. 4, and show a polyhedral structure with smooth surfaces. A TEM image of RB-61Si is shown in Fig. 5. It is clear that nanorods retaining their original shape and size are incorporated within a thin film, indicating that the aggregation behavior of RB was not influenced by the sol–gel process. In a control experiment with TEOS but no GPTMS, nanorods were not observed by TEM, further proving that RB nanorods were successfully encapsulated and stabilized within silica in a sol–gel process using TEOS and GPTMS. GPTMS offered the stabilization role for RB nanorod due to its easy reactivity with RB molecule and hence the subsequent beneficialness for silica encapsulation from TEOS. In addition, the non-protic character of the pending group of GPTMS may also contribute to the stabilization of RB nanorod by improving the compatibility of RB nanorod with THF.

Zeta-potential measurements were also carried out for RB-61 (pH 2.7) and RB-61Si (pH 3.2). The zeta potential of the nanorods changed from 1.05 mV before to −8.38 mV after sol–gel treatment. This further confirms that dye aggregates were encapsulated in a silica layer via electrostatic interaction, since silica particles are negatively charged (pI ~ 2 [33–35]) and RB molecules are positively charged at pH 3.2.

Fig. 6 shows SAED patterns of an uncoated RB nanorod and a silica-encapsulated RB nanorod. The sharp electron reflection spots reveal that the nanorod is a single crystal (Fig. 6a). A series of concentric circles were detected in the SAED pattern of silica-encapsulated RB nanorod, along with a single-crystal lattice (Fig. 6b), which is attributed to the random orientation of silica. Therefore, the SAED patterns confirm that RB nanorods were successfully coated with a silica layer.

The mechanism of formation of RB nanorods can be deduced from the structure of RB molecules. The RB molecule has two alkylated amino groups, one with a positive charge on the N atom as an electron acceptor and the other with a lone electron pair on the N atom (see Fig. 2). Owing to their planar structures, an approximate face-to-face arrangement of the donor–acceptor (D–A) pair is expected under specific conditions. The arrangement of RB molecules under various conditions is presented in Fig. 7. In aqueous solution, the positive charge on the N atom tends to transfer to the xanthene ring, followed by rotation between them, resulting in a twisted intramolecular charge transfer (TICT) state [36]. Besides, dye molecules are ionized in aqueous media, leading to strong electrostatic repulsion forces between RB molecules. As a consequence, RB molecules are randomly arranged to form disordered aggregates, as schematically depicted in Fig. 7b. However, in THF-rich media, the high positive entropy due to THF addition leads to rearrangement of solute and solvent molecules to yield better order. On the other hand, due to the weak polarity of THF, the positive charge on the N atom of one RB molecule tends to

Fig. 5. TEM image of RB-61Si.

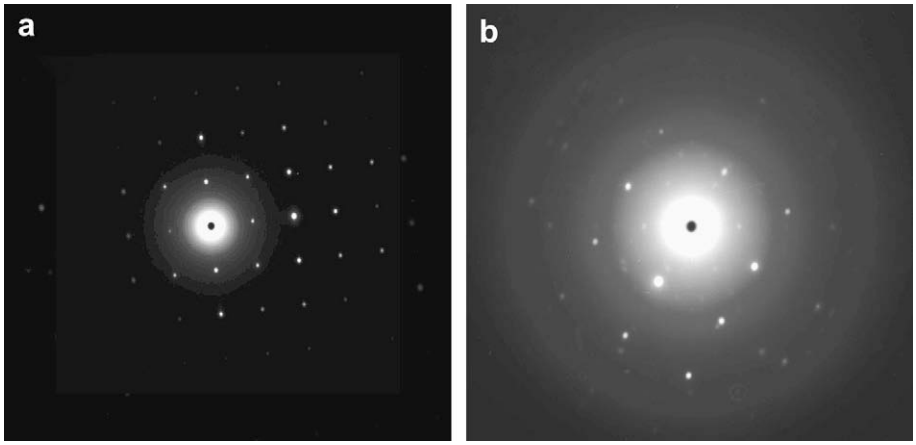

Fig. 6. SAED patterns of (a) single RB nanorod and (b) silica-encapsulated RB nanorods.

transfer to the lone electron pair on the N atom of an adjacent molecule instead of intramolecular charge transfer, restricting the rotation of the groups and leading to a face-to-face arrangement between RB molecules, as illustrated in Fig. 7c. In addition, the decrease in electrostatic repulsion forces between RB molecules also facilitates the aggregation of RB molecules in THF-rich media. Consequently, well-organized RB nanorods are obtained in mixtures of water and THF.

3.3. Leaching experiments

Immersion experiments on dye-doped glass in H_2O, HCl, ethanol and NaOH were conducted to test the leachability of silica-encapsulated RB aggregates. The absorption spectra of dye-doped glass and various leachates are presented in Fig. 8. The color change of leachates is shown in Fig. 9. Fig. 8 shows that the spectrum of dye-doped silica glass showed similar absorption to that of dye aggregates in solution (Fig. 1b). The leachates showed almost no absorption after glass immersion in H_2O, HCl and ethanol, and only a very weak absorption peak at ~550 nm was detected for NaOH leachate, which might be caused by the poor alkali resistance of silica. In agreement with the spectral data, the H_2O, HCl and ethanol leachates were almost colorless, whereas the NaOH leachate was light pink (Fig. 9). Similar leaching behavior was observed in the control experiments with low RB concentration (10^{-5} M), wherein only RB molecules were entrapped in silica matrix. Therefore, it can be concluded that non-leachability in H_2O, HCl and ethanol should have resulted from the protection of silica matrix instead from the insolubility of RB nanorod in H_2O, HCl and ethanol.

3.4. Emission spectra

Fig. 10 shows emission spectra of RB solution and dispersions at high concentration. The aqueous RB solution exhibits a low-intensity peak, whereas RB dispersions exhibit a gradual increase in peak intensity and an obvious blue shift with increasing THF

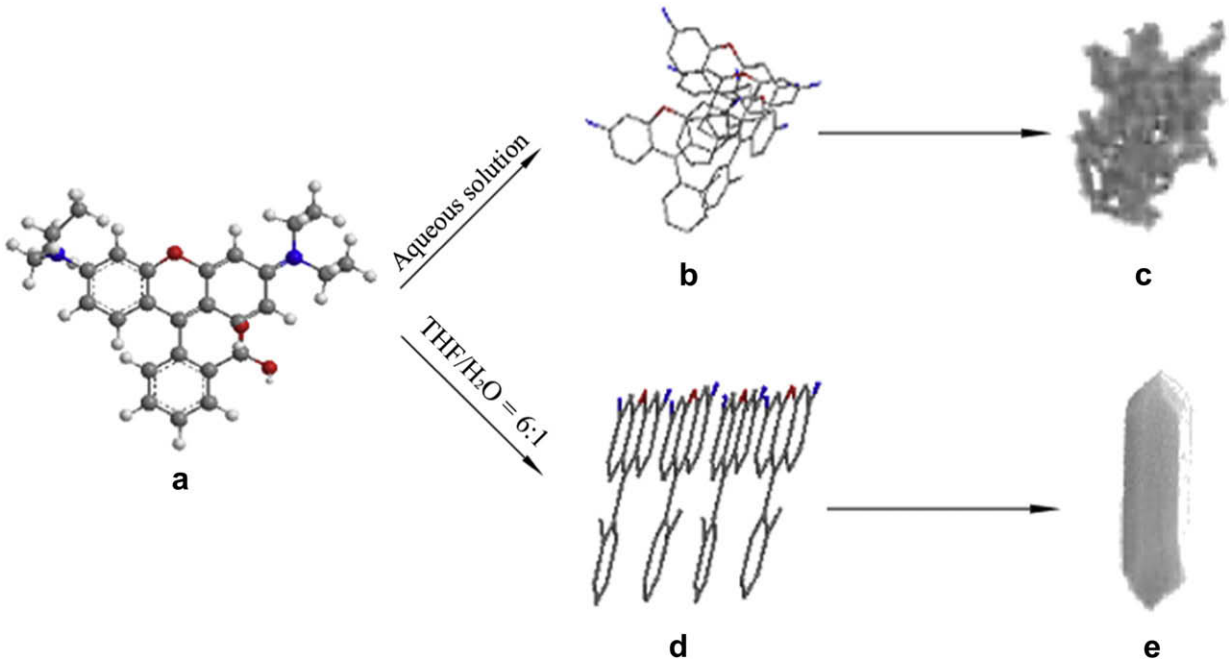

Fig. 7. Schematic for formation process of RB aggregates under various conditions. (a) Single RB molecule, (b) random arrangement of RB molecules in aqueous solution, (c) face-to-face arrangement of RB molecules in the mixture of water and THF, (d) amorphous RB aggregates, and (e) the formed RB nanorod.

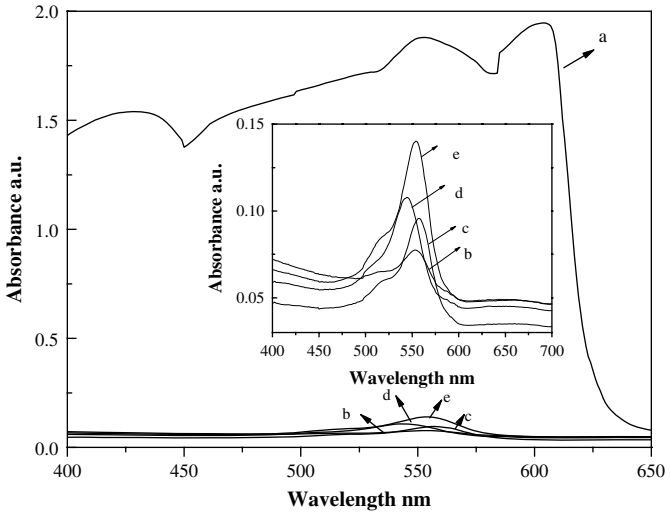

Fig. 8. Absorption spectra of (a) RB-doped glass and the leachates of (b) H_2O, (c) HCl, (d) ethanol, and (e) NaOH. Inset: absorption spectra of the leachates in an enlarged scale.

amount; the silica-encapsulated RB has even higher peak intensity than the corresponding RB-61.

It is well known that fluorescent quenching results from non-radiative deactivation of excited dye molecules. For RB molecules, it has been reported that non-radiative deactivation is mainly due to internal conversion via a twisted intramolecular charge transfer (TICT). The TICT state of RB molecules is strongly favored in aqueous solution, which explains the low emission intensity of the aqueous RB solution. On THF injection into aqueous RB solution, well-organized RB aggregates were formed that contributed to the increase in emission intensity by restricting the rotation of groups of RB molecules and formation of the TICT state. The extremely high emission intensity for silica-encapsulated RB nanorods can be ascribed to the restriction of charge transfer by the silica shell.

Similar to the absorption spectra, the blue shifts in emission spectra for RB in binary solvent may be explained by the disruption of solute–solvent interactions and strong intramolecular interactions due to THF addition.

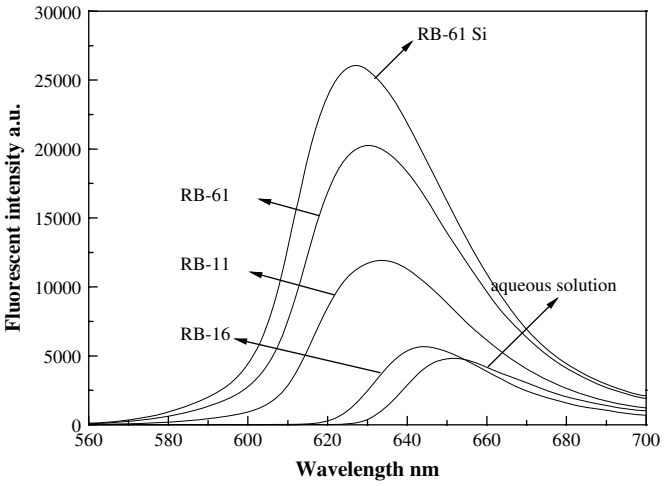

Fig. 10. Emission spectra of RB aqueous and dispersions at high concentration (1×10^{-2} M).

3.5. Photostability

Most fluorescent organic dyes fade quickly when exposed to UV irradiation, resulting in serious attenuation of the absorbance and emission intensities [23]. Fig. 11 presents the relative emission intensities of the aqueous RB solution, RB-61, and RB-61Si as a function of UV irradiation time. The emission intensity of the aqueous RB solution quickly decreased as UV irradiation time was extended. However, the fluorescent fading of RB-61 was much slower than that of the aqueous RB solution, and the slowest fading was observed for RB-61Si, indicating the best photostability of RB-61Si.

The single-photon photobleaching mechanism can explain the change in photostability of RB in different states. [37] A dye molecule can be oxidized by reactive singlet oxygen and this photo-oxidation process mainly causes fading of the dye molecules under UV irradiation. Therefore, all organic dyes exhibit higher photo-stability in an oxygen-depleted atmosphere. Owing to the formation of well-defined aggregates in the THF/H_2O mixture, oxygen

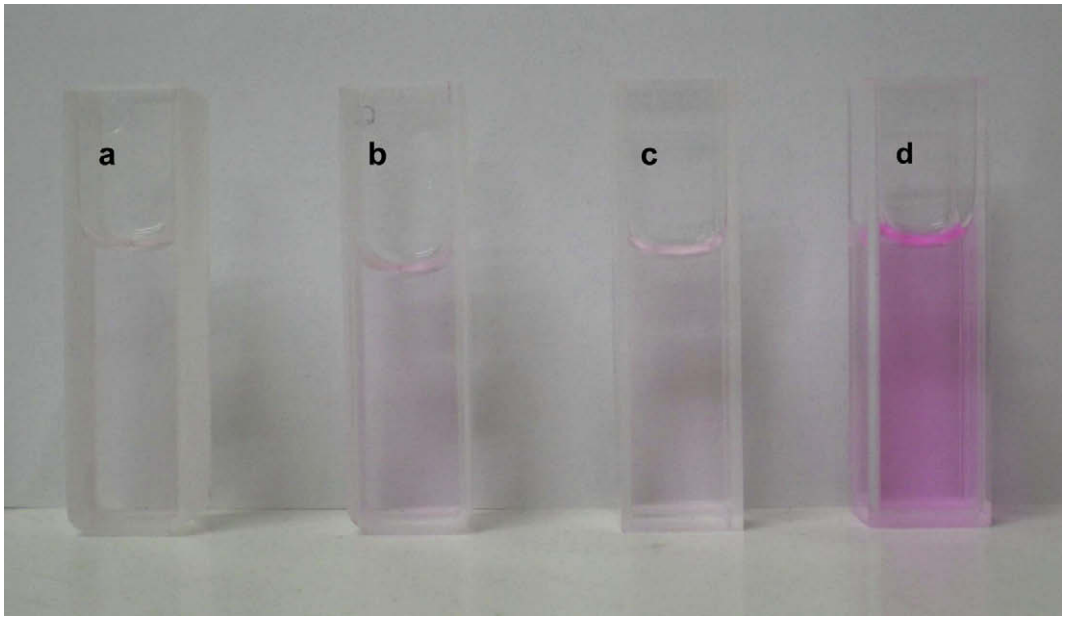

Fig. 9. The appearances of the leachates of (a) H_2O, (b) HCl, (c) ethanol, (d) NaOH.

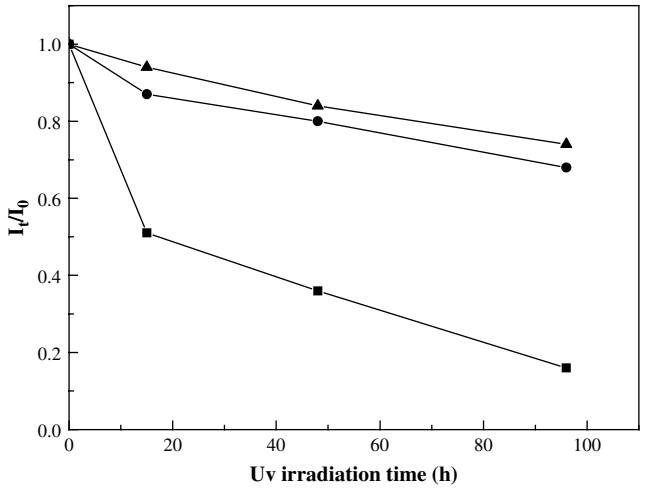

Fig. 11. The relative emission intensities of aqueous RB solution (■), RB-61 (●) and RB-61Si (▲) as a function of UV irradiation time (I_t and I_0 denote the height of the emission peak at UV irradiation time of t and 0, respectively. RB concentration = 1×10^{-2} M).

diffusion in this system is inhibited. As a result, the photostability of RB in the binary solvent is higher than that in aqueous solution. When encapsulated in silica, the silica shell can protect RB nanorods from oxygen and thus they exhibit enhanced photostability.

4. Conclusions

The self-assembly behavior, spectroscopic properties and stability of RB dispersions at comparatively high concentration were investigated by tuning the THF/H_2O volume ratio. UV–vis spectra observed for RB at comparatively high concentration were quite different from those in dilute systems due to the formation of trimers and polymers. As the amount of THF increased, the maximum position of the peak was gradually blue-shifted. At relatively high THF/H_2O ratios, rod-like nanocrystals of RB with higher fluorescent intensity were formed. TEM, zeta-potential measurement and SAED patterns indicated that RB nanorods were successfully encapsulated in a silica layer using a sol–gel process with TEOS and GPTMS. Owing to the protection conferred by the silica matrix, the RB nanorods exhibit strong fluorescent emission, high non-leachability in polar solvents and photostability under UV irradiation. Based on the results of the present study, supramolecular architectures with a well-organized nanostructure of other organic dyes could be constructed at high concentrations and further stabilized for various applications.

Acknowledgements

Financial support for this research by the Foundation of Science and Technology of Shanghai (07DJ14004), the Shanghai Leading Academic Discipline Project (B113), the Shanghai Excellent Leader of Academic Discipline Project, and the Shuguang Scholar-Tracking Foundation of Shanghai is greatly appreciated.

References

[1] Arunkumar E, Forbes CC, Smith BD. Improving the properties of organic dyes by molecular encapsulation. Eur J Org Chem 2005;2005:4051–9.
[2] Würthner F, Yao S. Dipolar dye aggregates: a problem for nonlinear optics, but a chance for supramolecular chemistry. Angew Chem 2000;112:2054–7.
[3] Tian ZY, Chen Y, Yang WS, Yao JN, Zhu LY, Shuai ZG. Low-dimensional aggregates from stilbazolium like dyes. Angew Chem 2004;116:4152–5.
[4] Horn D, Rieger J. Organic nanoparticles in the aqueous phase – theory, experiment, and use. Angew Chem Int Ed 2001;40:4330–61.
[5] Liu MH, Kira A, Nakahara H. Two-dimensional aggregation of a long-chain thiacarbocyanine dye monolayer on polyanion subphases. J Phys Chem 1996;100:20138–42.
[6] Khazraji AC, Hotchandani S, Das S, Kamat PV. Controlling dye (merocyanine-540) aggregation on nanostructured TiO_2 films. An organized assembly approach for enhancing the efficiency of photosensitization. J Phys Chem B 1999;103:4693–700.
[7] Würthner F, Yao S, Debaerdemaeker T, Wortmann R. Dimerization of merocyanine dyes. Structural and energetic characterization of dipolar dye aggregates and implications for nonlinear optical materials. J Am Chem Soc 2002;124:9431–47.
[8] Mulo J. Dimeric properties of Rhodamine B in glycerol, ethylene glycol, and acetic acid. J Phys Chem 1976;80:1342–6.
[9] Selwyn JE, Steinfeld JI. Aggregation equilibria of xanthene dyes. J Phys Chem 1972;76:762–74.
[10] Aguilera OV, Nechers DC. Aggregation phenomena in xanthene dyes. Acc Chem Res 1989;22:171–7.
[11] Dakiky M, Němcova. Aggregation of *o,o′*-dihydroxyazo dyes-1. Concentration, temperature, and solvent effect. Dyes Pigments 1999;40:141–50.
[12] Place I, Perlstein J, Penner TL, Whitten DG. Stabilization of the aggregation of cyanine dyes at the molecular and nanoscopic level. Langmuir 2000;16:9042–8.
[13] Berlepsch HV, Böttcher C, Dähne L. Structure of J-aggregates of pseudoisocyanine dye in aqueous solution. J Phys Chem B 2000;104:8792–9.
[14] Zhang YZ, Xiang JF, Tang YL, Xu GZ, Yan WP. Aggregation behaviour of two thiacarbocyanine dyes in aqueous solution. Dyes Pigments 2008;76:88–93.
[15] Yao H, Kobayashi S, Kimura K. Self-assembly of acridine orange dye at a mica/solution interface: formation of nanostripe supramolecular architectures. J Colloid Interface Sci 2007;307:272–9.
[16] Tian ZY, Zhang YZ, Zhang YL, Peng AD, Ma Y, Chen Y, et al. On the formation of nanostructures from stilbazolium-like dyes. J Nanopart Res 2006;8:65–77.
[17] Gesquiere AJ, Uwada T, Asahi T, Masuhara H, Barbara PF. Single molecule spectroscopy of organic dye nanoparticles. Nano Lett 2005;5:1321–5.
[18] Avnir D, Levy D, Reisfeld R. The nature of the silica cage as reflected by spectral changes and enhanced photostability of trapped Rhodamine 6G. J Phys Chem 1984;88:5956–9.
[19] Monte FD, Levy D. Formation of fluorescent Rhodamine B J-dimers in sol–gel glasses induced by the absorption geometry on the silica surface. J Phys Chem B 1998;102:8036–41.
[20] Monte FD, Mackenzie JD, Levy D. Rhodamine fluorescent dimers adsorbed on the porous surface of silica gels. Langmuir 2000;16:7377–82.
[21] Ferrer ML, Monte FD, Levy D. Rhodamine 19 fluorescent dimers resulting from dye aggregation on the porous surface of sol–gel silica glasses. Langmuir 2003;19:2782–6.
[22] Gutiérrez MC, Hortigüela MJ, Ferrer ML, Monte FD. Highly fluorescent Rhodamine B nanoparticles entrapped in hybrid glasses. Langmuir 2007;23:2175–9.
[23] Negishi N, Fujino M, Yamashita H, Fox MA, Anpo M. Photophysical properties and photochemical stability of Rhodamine B encapsulated in SiO_2 and Si–Ti binary oxide matrices by the sol–gel method. Langmuir 1994;10:1772–6.
[24] Pouxviel JC, Dunn B, Zink JI. Fluorescene study of aluminosilicate sols and gels doped with hydroxy trisulfonated pyrene. J Phys Chem 1989;93:2134–9.
[25] Gilliland JW, Yokoyama K, Yip WT. Effect of coulombic interaction on rotational mobility of guests in sol–gel silicate thin films. Chem Mater 2004;16:3949–54.
[26] Ogawa M, Kawai R, Kuroda K. Adsorption and aggregation of a cationic cyanine dye on smectites. J Phys Chem 1996;100:16218–21.
[27] Bujdák J, Iyi N. Molecular aggregation of Rhodamine dyes in dispersions of layered silicates: influence of dye molecular structure and silicate properties. J Phys Chem B 2006;110:2180–6.
[28] Bujdák J, Iyi N, Sasai R. Spectral properties, formation of dye molecular aggregates, and reaction in Rhodamine 6G/layered silicate dispersions. J Phys Chem B 2004;108:4470–7.
[29] Chang TL, Cheung HC. Solvent effects on the photoisomerization rates of the zwitterionic and the cationic forms of Rhodamine B in protic solvents. J Phys Chem 1992;96:4874–8.
[30] Ferreira JAB, Costa SMB, Ferreira LFV. Activated radiationless decay of Rhodamine 3B: polarity and friction effects. J Phys Chem A 2000;104:11909–17.
[31] Silva AAD, Flor J, Davolos MS. Rhodamine B-containing silica films from TEOS precursor: substrate surface effects detected by photoluminescene. Surf Sci 2007;601:1118–22.
[32] Ramette RW, Sandell EB. Rhodamine B equilibria. J Am Chem Soc 1956;78:4872–7.
[33] Hench LL, West JK. The sol–gel process. Chem Rev 1990;90:33–72.
[34] Wen J, Wilkes GL. Organic/inorganic hybrid network materials by the sol–gel approach. Chem Mater 1996;8:1667–81.
[35] Yuan JJ, Zhou XS, Wu LM, You B. Organic pigment particles coated with titania via sol–gel process. J Phys Chem B 2006;110:388–94.
[36] Arbeloa FL, Arbeloa TL, Estévez MJT, Arbeloa IL. Photophysics of Rhodamines. Molecular structure and solvent effects. J Phys Chem 1991;95:2203–8.
[37] Gilliland JW, Yokoyama K, Yip WT. Solvent effect on mobility and photostability of organic dyes embedded inside silica sol–gel thin films. Chem Mater 2005;17:6702–12.